Molecular Vision 2015; 21:930-938 <http://www.molvis.org/molvis/v21/930>
Received 17 May 2015 | Accepted 22 August 2015 | Published 25 August 2015

Experimental endostatin-GFP gene transfection into human retinal vascular endothelial cells using ultrasound-targeted cationic microbubble destruction

Yan Xu,[1] Zongyuan Xie,[2] Yu Zhou,[1] Xiyuan Zhou,[3] Pan Li,[1] Zhigang Wang,[1] Qunxia Zhang[1]

[1]Institute of Ultrasound Imaging and Department of Ultrasound, Second Affiliated Hospital of Chongqing Medical University; Chongqing Key Laboratory of Ultrasound Molecular Imaging, Chongqing, P.R. China; [2]Department of Anesthesiology, Chongqing City Hospital of Traditional Chinese Medicine, Chongqing, P. R. China; [3]Department of Ophthalmology, Second Affiliated Hospital of Chongqing Medical University, Chongqing, P. R. China

Purpose: The purpose of this study was to investigate whether ultrasound-targeted cationic microbubble destruction could effectively deliver endostatin-green fluorescent protein (ES-GFP) plasmids to human retinal vascular endothelial cells (HRECs).

Methods: Cationic microbubbles (CMBs) were prepared and then compared with neutral microbubbles (NMBs) and liposomes. First, the two types of microbubbles were characterized in terms of size and zeta potential. The cell viability of the HRECs was measured using the 3-(4,5-dimthylthiazol-2-yl)-2,5 diphenyl-tetrazolium bromide (MTT) assay. The transcription and expression of endostatin, VEGF, Bcl-2, and Bcl-xl were measured via quantitative real-time PCR (qPCR) and western blotting, respectively.

Results: CMBs differed significantly from NMBs in terms of the zeta potential, but no differences in size were detected. Following ultrasound-targeted microbubble destruction (UTMD)-mediated gene therapy, the transcription and expression of endostatin were highest in the CMB group ($p<0.05$), while the transcription and expression of VEGF, Bcl-2, and Bcl-xl were lowest compared with the other groups. Moreover, the inhibition of HREC growth was enhanced following treatment with CMBs compared with NMBs or liposomes in vitro ($p<0.01$).

Conclusions: This study demonstrated that ultrasound-mediated cationic microbubbles could enhance the transfection efficiency of ES-GFP, which had obvious impacts on the inhibition of the growth process of HRECs in vitro. These results suggest that the combination of UTMD and ES-GFP compounds might be a useful tool for gene therapy targeting retinal neovascularization.

Retinal neovascularization (RNV) is an eye disease that can cause retinal detachment and even lead to blindness. RNV includes conditions such as diabetic retinopathy, central retinal vein occlusion, and retinopathy of prematurity. Existing treatments are limited to techniques such as laser photocoagulation and surgery [1]. Although these treatments exhibit a certain curative effect, there are many side effects and limitations. Therefore, the search for a new and effective treatment has become a research focus in ophthalmology. The pathogenesis of RNV has been confirmed to be highly related to the balance of proangiogenic and antiangiogenic factors [2], and the retinal endothelial cell is a major participant in RNV [3]; thus, the prevention of new blood vessel growth is the key to the treatment of these diseases.

Correspondence to: Qunxia Zhang, Institute of Ultrasound Imaging and Department of Ultrasound, Second Affiliated Hospital of Chongqing Medical University; Chongqing Key Laboratory of Ultrasound Molecular Imaging, Chongqing 400010, China; Phone: +86-23-63693602; FAX: +86-23-63822696; email: ziyan0835@sina.com

In this study, we selected the endostatin gene (Gene ID: 80781, OMIM 120328) due to its excellent antiangiogenic ability. Endostatin is the 20 kDa C-terminal fragment of collagen XVIII produced by hemangioendotheliomas, which functions as an angiogenesis inhibitor. Endostatin specifically inhibits endothelial proliferation and potently inhibits angiogenesis and tumor growth [4]. Bai [5] reported that endostatin could offer an innovative pharmaceutical strategy for the prevention of retinal neovascularization. However, the amount of endostatin protein required to achieve a therapeutic effect is high and represents a significant expense. Furthermore, endostatin is not stable, which limits its widespread clinical application. Thus, gene therapy may be the best way to exploit the advantages of endostatin in antiangiogenesis [6-9].

Gene therapy offers a novel approach for the prevention and treatment of many refractory diseases but is not yet commonly used in clinical cases due to various problems [10]. Effective gene therapy requires high gene transfection efficiency and protein expression. Ultrasound-targeted microbubble destruction (UTMD) is a noninvasive gene transfer

technology that provides a new means for carrying out gene therapy [11]. UTMD facilitates the cellular uptake of DNA via the process of sonoporation, which refers to the formation of transient cell membrane microperforations induced through ultrasonic cavitation. Microbubbles serve as cavitation nuclei that can reduce the ultrasound energy threshold necessary for sonoporation and enhance ultrasound energy deposition in tissues, thus increasing intracellular gene delivery [12-14]. The main biologic limitation of the technique is its low transfection efficiency; thus, several studies have focused on how to overcome this problem.

Microbubbles carry genes through electrostatic adsorption. Nucleic acids and the cell surface are negatively charged; therefore, the most commonly used microbubbles present either a net neutral or slightly negative surface charge, which minimizes the interaction of the microbubbles with cellular or molecular components in the plasma [15]. To further enhance the efficiency of gene delivery, recent studies have developed cationic microbubbles (CMBs) that exhibit a positive surface charge and are capable of electrostatically binding to negatively charged nucleic acids and cells [16-20]. Several studies have reported that the use of CMBs could increase the gene-carrying capacity and enhance gene transfer.

In previous studies, we screened the parameters of UTMD to ensure the safety of the animals' retina, and hematoxylin and eosin (H&E) staining showed that the rat retinal and choroidal structures were the same as those of the normal rat. We found that the therapeutic gene could be delivered by UTMD to the retina and inhibited the development of choroidal neovascularization [21]. Thus far, we have not found obvious side effects in the clinical use of sonoporation and gene delivery to the retina with microbubbles.

METHODS

Cell culture: Human retinal vascular endothelial cells (HRECs) were purchased from TongPai Biotechnology Co., Ltd (Shanghai, China) and grown in RPMI-1640 medium (Gibco, San Jose, CA) supplemented with 10% fetal bovine serum (FBS; v/v), 100 µg/ml streptomycin (Sigma, St. Louis, MO), and 100 U/ml penicillin (Sigma) at 37 °C in a 5% CO_2 humidified atmosphere. The cell numbers for all experiments were determined with a hemocytometer.

Plasmid preparation: A eukaryotic coexpression vector (pEZ-M46-ES) encoding green fluorescent protein (GFP) was obtained from GeneCopoeia™ Co. (Guangzhou, China). The GFP sequence was directly amplified via PCR using the upstream and downstream primers 5′-ATC GTT CGA ACC ATG GCG CCG AGG TGC CCC TGG CC-3′ and 5′-ATC GTG CGG CCG CAC TCG AGG TAC TTG GAG GCA GTC ATG AAG CTG T-3′, respectively. The recombinant plasmid was designated ES-GFP. The plasmids were grown under kanamycin selection in the host strain DH5α and purified through alkaline lysis and chromatographic methods using an EndoFree kit (Qiagen, Valencia, CA) at a concentration of 500 ng/µl. The concentration of the plasmid DNA was determined via spectrophotometry (NanoDrop 2000/2000C, Thermo Scientific, Waltham, MA).

CMB and NMB preparation and characterization: The neutral microbubbles (NMBs) consisted of 5 mg dipalmitoyl phosphatidylcholine (DPPC) and 2 mg 1,2-dipalmitoyl-sn-glycero-3-phosphoethanol-amineN-[methoxy(polyethylene glycol)-2000] (DSPE-PEG2000). The CMBs consisted of 5 mg DPPC, 2 mg 1,2-distearoyl-sn-glycero-3-phosphoethanolamine-N-[biotinyl (polyethylene glycol)-2000] (DSPE-PEG2000-Biotin), and 1 mg 3-(N-(N',N'-dimethylaminoethane)carbamoyl)cholesterol (DC-Chol). All chemicals were obtained from Avanti Polar Lipids (Alabaster, AL). They were dissolved in PBS (1X; 137 mM NaCl, 2.7 mM KCl, 10 mM Na_2HPO_4, 2 mM KH_2PO_4, pH 7.4) at a final volume of 0.5 ml in 1.5-ml vials. The vials were incubated at 37°C for 30 min. The headspace in each vial was filled with perfluoropropane gas, and the vial was then mechanically shaken for 45 s using a dental amalgamator (Medical Apparatus and Instrument, YJT, Shanghai, China). This solution was diluted with 0.5 ml PBS and sterilized through Co60 irradiation. The density of the cationic microbubbles was 1×10^9/ml.

Both types of microbubbles were stable in suspension for up to 1 month at 4 °C. The size distribution and zeta potential were analyzed in Opti-MEM (Invitrogen, Carlsbad, CA) using a laser particle size analyzer system (Zetasizer 3000HS; Malvern, UK).

Assessment of plasmid binding to microbubbles: The strategy for evaluating the amount of plasmid DNA that can bind to microbubbles followed the method described by Panje et al. [22]. Briefly, 5×10^8 NMBs and CMBs were incubated with varying doses of ES-GFP plasmids (10, 20, and 40 µg) in Opti-MEM for 15 min to allow spontaneous electrostatic charge-coupling between the DNA and the microbubbles. Then the samples were centrifuged at 400 ×*g* for 4 min to form two phases: The upper layer contained microbubbles with bound DNA, and the lower layer contained unbound DNA. The lower layer was collected and centrifuged at 14,000 ×*g* for 5 min using 0.45-µm centrifugation filters to remove MB shell contaminants. The concentration of unbound DNA was determined via spectrophotometry (NanoDrop 2000/2000C, Thermo Scientific) and by multiplying the total sample volume obtained by the total amount of unbound DNA. The amount of bound DNA was calculated by subtracting

the amount of unbound DNA from the total amount of DNA added initially. By increasing the initial amount of DNA, the maximum amount of bound DNA was obtained, which was regarded as the loading capacity for 5×10^8 microbubbles. All experiments were performed in triplicate.

Gene transfer: ES-GFP plasmids grown in Escherichia coli were purified and suspended in 2.5 mM Tris-HCl (pH 8.5) at a concentration of 1.0 µg/µl. Five micrograms of plasmids (5 µl with 5×10^8 of a CMB or NMB suspension were gently blended, and the mixture was gently incubated for a few minutes at 4 °C to achieve adhesion. Cells were transfected with the ES-GFP vector using Lipofectamine 2000 (Invitrogen, Carlsbad, CA). Five micrograms of plasmids were gently blended with 45 µl of RPMI-1640 medium or 3 µl of liposome plus 47 µl of RPMI-1640 medium, and these two components were mixed at room temperature for 20 min. Gene transfer (UGT 1025 type, Chongqing, China) was performed by the Ultrasonographic Image Research Institute of Chongqing Medical University. The following parameters were used for the ultrasound treatment of the HRECs: continuous wave, 1 MHz, 1 W/cm^2, 20% duty cycle, 1 min, and a 10% concentration of microbubbles. Cultured HRECs were divided into four groups: (1) control (no treatment), (2) ES-GFP plasmid with NMBs and ultrasound (hereafter referred to as the NMB group), (3) ES-GFP plasmids with liposomes (hereafter referred to as the liposome group), and (4) ES-GFP plasmids with CMBs and ultrasound (hereafter referred to as the CMB group). The second and fourth groups of cells were grown in an Opticell for 24 h before transfection. The Opticell contained two layers of parallel breathable polystyrene (PS) film with a special surface treatment, making it suitable for cell growth. The total size of the training device was the same as a traditional microporous plate. After the microbubble composite plasmid was injected, the Opticell was inverted to allow full contact between the microbubbles and the cells to maximize the effect. After incubation for 6 h at 37 °C with 5% CO_2, the compound solution was replaced with 500 µl of fresh media containing 10% fetal bovine serum and 1% penicillin/streptomycin. The cells were cultured for another 24 h, and the reporter ES-GFP expression was analyzed. All transfection experiments were performed in triplicate.

MTT assay: The influence of all treatment factors on the cell viability of the HRECs was assessed using the 3-(4,5-dimthyl-thiazol-2-yl)-2,5 diphenyl-tetrazolium bromide (MTT) assay. After transfection, all groups of HRECs were collected and immediately seeded into 96-well plates at a density of 1×10^4 cells per well. When the cells had grown to approximately 60–80% confluency, the old medium was replaced with 200 µl of RPMI-1640 without FBS and penicillin/streptomycin. The cells were then incubated at 37 °C and inspected daily for 5 days. Cell growth was determined by adding 20 µl of MTT (5 µg/ml) to each well, followed by incubation for an additional 4 h at 37 °C. The supernatants were discarded, and 150 µl of dimethyl sulfoxide was added. The absorbance was determined via spectrophotometry using a wavelength of 570 nm, with 630 nm as a reference. All experiments were performed in triplicate.

qPCR: The total RNA was extracted via phenol-chloroform extraction with ethanol precipitation using TRIzol (Life Technologies, Gaithersburg, MD). The integrity of the RNA was determined on 1.5% agarose gels containing ethidium bromide. Reverse transcription to cDNA was performed using the Takara PrimeScript™ RT Reagent Kit (AMV; Takara, Tokyo, Japan) with Bio-Rad iQ5. The reaction conditions were as follows: 25 °C for 10 min, 42 °C for 50 min, and 85 °C for 5 min. The quantitative real-time PCR (qPCR) amplification conditions were as follows: 94 °C for 4 min; 35 cycles of 94 °C for 20 s, 60 °C for 30 s, and 72 °C for 30 s; and finally, the signal was measured at 72 °C. The bands were normalized to β-actin. The primer sequences are provided in Table 1.

Table 1. The primer sequences of endostatin, VEGF and BCl-2 BCl-Xl detected by qPCR

Detected gene	Primer sequences	
COL18A1 Endostatin	hCOL18A1F	GATTTGGCATGAGGGGAATG
	hCOL18A1R	AAGAAAGTCAAACGGAAACTGC
VEGF	hVEGFF	AATCGAGACCCTGGTGGACA
	hVEGFR	TGTTGGACTCCTCAGTGGGC
BCL-2	hBCL-2F	CCGAGATGTCCAGCCAGC
	hBCL-2R	CCCACCGAACTCAAAGAAGG
BCL-XL	hBCL-XLF	CTGAATCGGAGATGGAGACCC
	hBCL-XLR	AACTCGTCGCCTGCCTCC

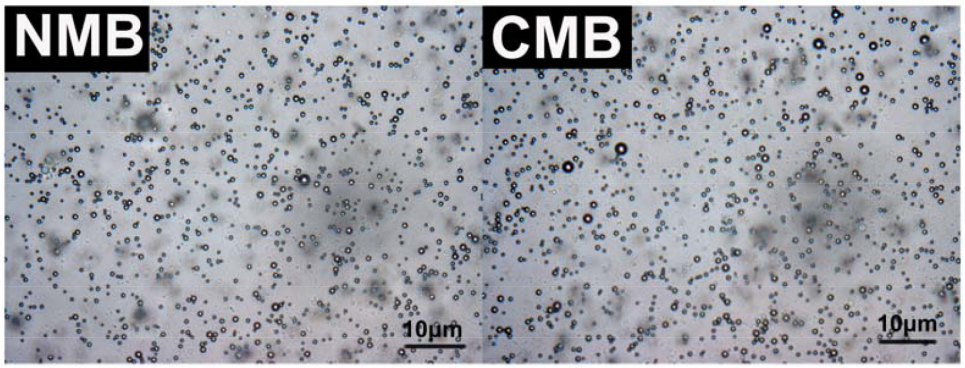

Figure 1. Characterization of microbubbles under a microscope. Bright-field images of the neutral microbubbles (NMBs) and the cationic microbubbles (CMBs). The images were acquired at 1,000X magnification, and the scale bar is set to 10 μm.

Western blot analysis: All HREC groups were collected 72 h after transfer. Briefly, the proteins were separated via sodium dodecyl sulfate–polyacrylamide gel electrophoresis (SDS–PAGE) in 12% (w/v) polyacrylamide gels and electrotransferred to Millipore polyvinylidene difluoride membranes (Millipore, Bedford, MA). The completion of the protein transfer from the gels to the membranes was verified by staining the gels with Coomassie Blue R-250. The membranes were blocked in Tris-buffered saline containing 0.05% Tween-20 and 5% nonfat dry milk for 60 min at room temperature. Then, the blots were incubated with a 1:1,000 dilution of a rabbit anti-human endostatin antibody (Abcam, London, UK), rabbit anti-human VEGF antibody (Abcam), or rabbit anti-human ES antibody (Abcam) for 1.5 h at room temperature in blocking solution. The membranes were washed in Tris-buffered saline and incubated with horseradish peroxidase-conjugated goat anti-rabbit immunoglobulin G (IgG; 1:3,000) in blocking solution for 1.5 h. The blots were examined using a chemiluminescent substrate (Santa Cruz Biotechnology, Santa Cruz, CA) according to the manufacturer's instructions. The protein bands were normalized to glyceraldehyde 3-phosphate dehydrogenase (GAPDH), and all of the blots were quantified using Quantity One software (Bio-Rad, Hercules, CA).

Statistical analysis: All of the data are expressed as the mean ± standard deviation and were analyzed using SPSS 17.0 software (SPSS Inc., Chicago, IL). Means showing $p<0.05$ were considered to be significantly different from one another. Comparisons between groups were performed using one-way ANOVA test. The least significant difference (LSD) and Student *t* tests were used for further comparisons.

RESULTS

Characterization of microbubbles: The characteristics of the CMBs and the NMBs are listed in Table 2. There were no significant differences in the mean diameters or concentrations of the NMBs and the CMBs, but the zeta potentials of the CMBs (+25.62±4.38 mV) were significantly higher than those of the NMBs (−2.78±1.56 mV; $p<0.001$). Inverted microscopy images of the NMBs and CMBs are shown in Figure 1.

Plasmid binding ability of microbubbles: Quantitative assessment of the DNA loading capacity of the NMBs and the CMBs revealed significantly higher plasmid binding abilities for the CMBs compared with the NMBs at every dose. As the number of added plasma molecules increased, the amount of plasmids bound to the CMBs increased as well. However, no further increases in the amount of plasmids bound to the CMBs was observed when 40 μg of plasmids was added to the microbubble solution. Therefore, the amount of plasmids that bound to the microbubbles when 40 μg of plasmid DNA was added to the microbubble solution was regarded as the saturated DNA loading capacity of 5×10^8 CMBs. The saturated DNA loading capacities of the NMBs and the CMBs were 19.02±0.76 μg and 5.01±0.74 μg, respectively (Figure 2, $p<0.05$). The zeta potential of the CMBs decreased slightly

Table 2. Summary of microbubble characteristics.

Micro-bubbles	Zeta-potential (mV)	Diameter (μm)	Concentration ($\times10^9$/ml)
NMB	−2.78±1.56	1.52±0.31	3.04±0.27
CMB	+25.62±4.38*	1.64±0.28	4.16±0.18

*$p<0.001$ relative to NMBs, n=3 per group

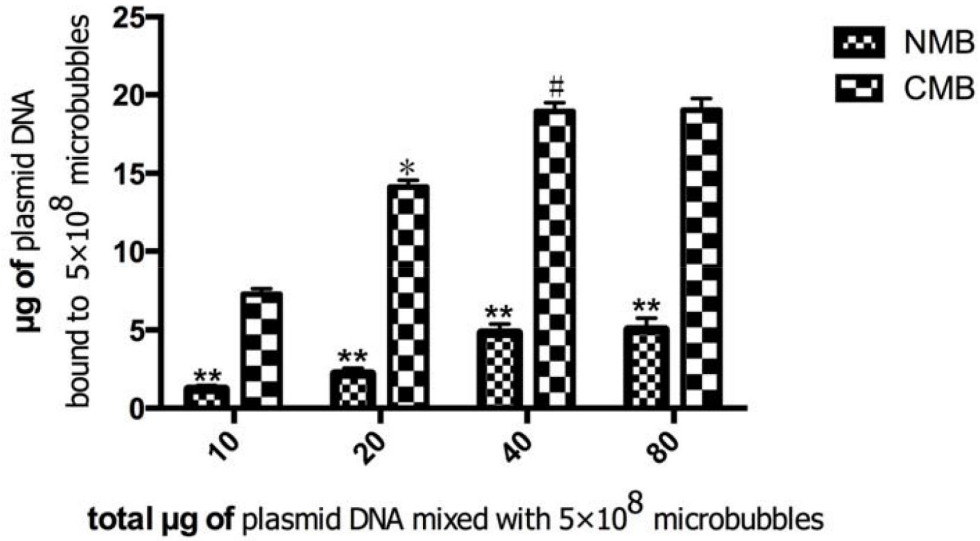

Figure 2. Quantitative assessment of DNA binding to NMBs and CMBs (n=3 per group). The DNA loading capacity of the cationic microbubbles (CMBs) was significantly higher than that of the neutral microbubbles (NMBs), regardless of the plasmid dosage in the microbubble solution (*p<0.01 relative to 10, 40, and 80 μg of plasmid DNA, within-group comparisons; #p>0.05 relative to 80 μg of plasmid DNA, within-group comparisons; **p<0.05 relative to the CMBs in each group).

(+16.32±3.28) after the bound DNA, but the size of the CMBs has no obvious change, and the size and the zeta potential of NMBs had no obvious change after the bound DNA.

MTT assay: The influence of all treatment factors on HREC cell viability was evaluated using the MTT assay. The cells treated with the ES-GFP plasmid together with NMBs and ultrasound, or with the ES-GFP plasmid with liposomes, or the ES-GFP plasmid with CMBs and ultrasound all underwent apoptotic-like cytological changes characterized by a loss of anchorage dependence and the assumption of a small spherical shape. The cells were collected and counted from day 1 through day 5, and the cell viability rate of the control group was 100%; the viability rate of the cells in each group was as shown in Figure 3. In multiple trials, the cell viability rate was observed to decrease significantly in the CMBs compared with the other groups.

qPCR: To evaluate the transcription of the ES-GFP gene after transfection into HRECs in vitro, the relative ratio of ES RNA in the treated and control HRECs was determined via qPCR at 48 h post-transfection (Figure 4A). To evaluate the effect of endostatin on VEGF, Bcl-2, and Bcl-xl expression, the relative ratios of VEGF, Bcl-2, and Bcl-xl RNA were also determined (Figure 4B–D). Following transfer, the transcription levels of the ES gene were highest in the CMB group (p<0.05 relative to the NMB and liposome groups, p<0.01 relative to the control group), while there was almost no difference between the NMB and liposome groups (p>0.05). With the increasing levels of ES RNA, the level of VEGF, Bcl-2, and

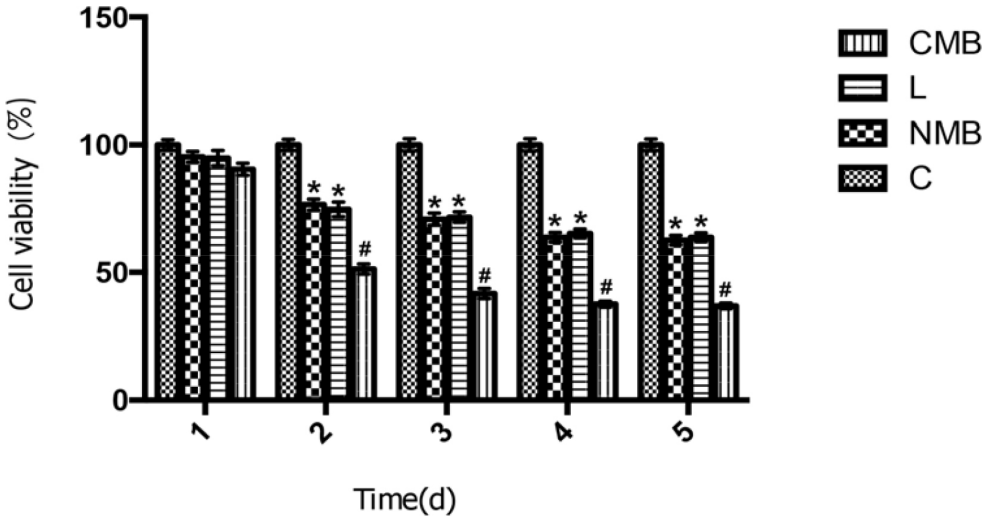

Figure 3. ES-GFP gene transfer suppresses HREC growth. Mean cell numbers were assessed for 5 consecutive days. Transfection with embryonic stem-green fluorescent protein (ES-GFP) using ultrasound-targeted cationic microbubble destruction caused a significant decrease in the human retinal vascular endothelial cell (HREC) cell viability rate compared with the other groups. (* p<0.05 relative to the control and cationic microbubble (CMB) groups, #p<0.01 relative to the control in every time point; n=6 per group).

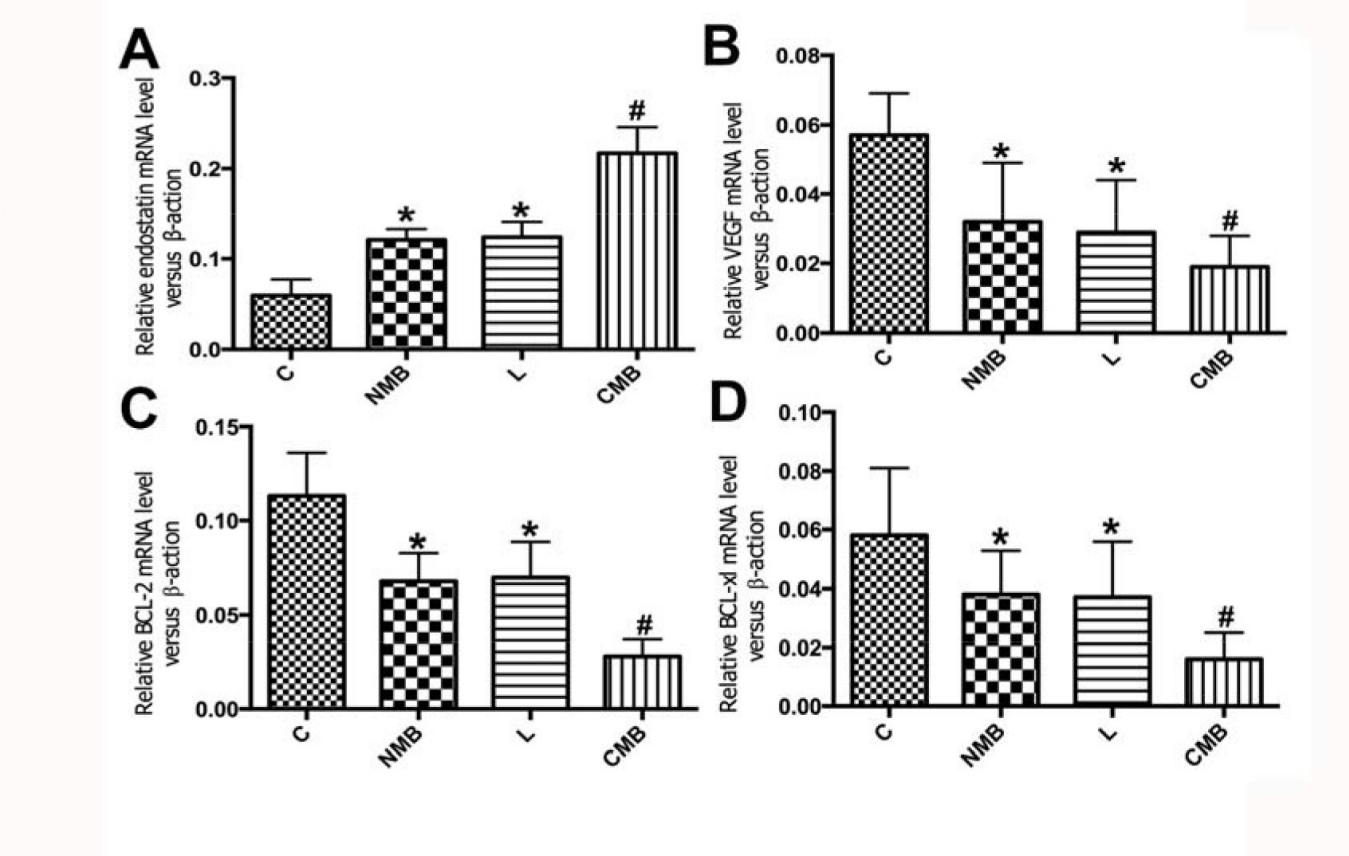

Figure 4. qPCR analysis of the transcription of the ES-GFP plasmid and the effect on VEGF, Bcl-2, and Bcl-xl. Endostatin (**A**), VEGF (**B**) Bcl-2(**C**), and Bcl-xl (**D**) mRNA levels were measured via quantitative real-time PCR (qPCR) 48 h after ultrasound-targeted microbubble destruction (UTMD)-mediated embryonic stem (ES) gene delivery. The levels of endostatin mRNA were significantly higher following cationic microbubble (CMB) delivery of the ES gene compared with the neutral microbubble (NMB), liposome, and control groups. VEGF, Bcl-2, and Bcl-xl mRNA levels were significantly lower following CMB delivery of the ES gene compared with the NMB, liposome, and control groups (* $p<0.05$ relative to the control and CMB groups, #$p<0.01$ relative to the control; n=6 per group).

Bcl-xl mRNA decreased (Figure 4). Thus, these effects may be due to the therapeutic effect induced by endostatin.

Western blotting: To evaluate the delivery of the ES-GFP gene into HRECs in vitro, the total amount of endostatin protein in the treated and control HRECs was determined with western blotting at 48 h post-transfection (Figure 5A). The endostatin protein level following transfer using CMBs and ultrasound was increased compared with the other groups. The difference in the endostatin protein levels between the CMB group and the other groups was significant ($p<0.05$ relative to the NMB and liposome groups, $p<0.01$ relative to the control group). However, the difference in the endostatin protein levels between the NMB group and the liposome group was not significant ($p>0.05$). To better evaluate the therapeutic effect following ES-GFP gene transfer, the protein levels of VEGF, Bcl-2, and Bcl-xl were examined. As the levels of the endostatin protein increased, the VEGF, Bcl-2, and Bcl-xl protein level decreased (Figure 5B-D), confirming the anti-angiogenesis and apoptosis effects of endostatin.

DISCUSSION

Retinal neovascularization is the leading cause of vision impairment worldwide. Angiogenesis is regulated by a balance between angiogenic and angiostatic regulators and is a continuous process that includes the activation, migration, and proliferation of vascular endothelial cells. Endostatin, one of the most potent antiangiogenesis agents identified to date, specifically inhibits vascular endothelial cell proliferation and migration. The effect of endostatin appears to be more significant than the effect observed following incubation with VEGF antibodies.

We previously reported that UTMD-mediated gene delivery (UMGD) with NMBs resulted in the successful transfection of genes into human retinal pigment epithelial

cells in vitro and into rat retinas and choroids in vivo, thus inhibiting the development of choroidal neovascularization [21]; however, the gene transfection efficiency was modest, similar to other researchers' reports [23,24]. As a promising noninvasive and non-viral strategy for gene therapy, UMGD has been continuously studied since its first appearance [25,26]. In recent years, studies have focused on improving transfection efficiency. Thus, CMBs were developed to enhance the loading capacity of DNA. In the present study, the CMBs were composed of DPPC, DSPE-PEG2000-Biotin, and DC-Chol in a specific ratio. We selected DC-Chol to obtain a positively charged surface of the microbubbles because it is one of the most efficient cationic lipids and has been widely used in drug delivery and gene transfection. We used DSPE-PEG2000-Biotin instead of DSPE-PEG2000 because we observed that this resulted in a higher concentration of CMBs and better stability.

Our previous work showed that most cells are able to survive under the conditions of 1 W/cm^2 sound intensity, 1 min irradiation time, 20% duty cycle, and 10% microbubble concentration. Therefore, we used these optimal conditions in this study.

In this study, CMBs bound more plasmid DNA compared with neutral microbubbles and enhanced gene transfer. The MTT values of the CMB group were dramatically reduced

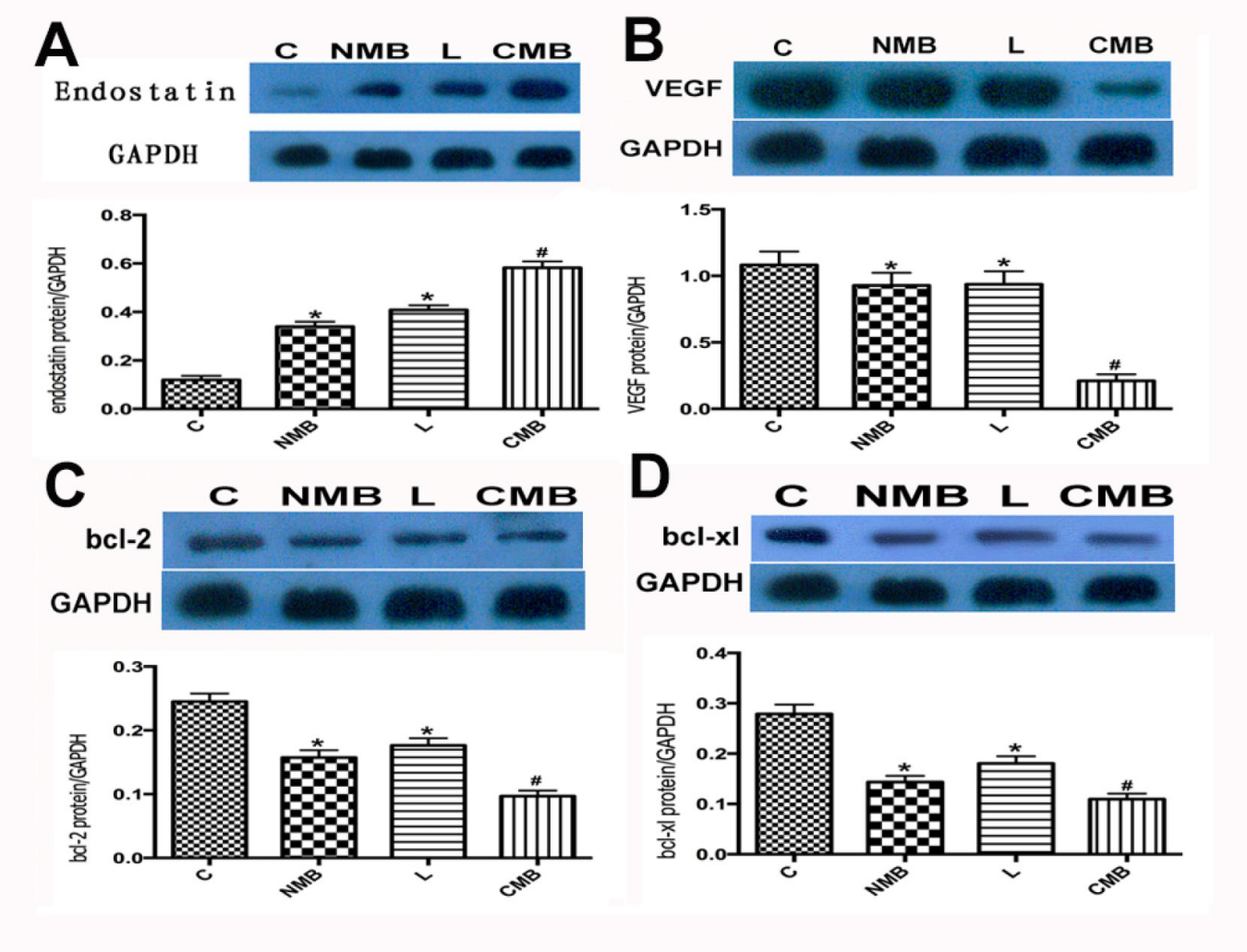

Figure 5. Western blot analyses of the expression of the endostatin protein and the effect on VEGF, Bcl-2, and Bcl-xl expression. Endostatin (**A**), VEGF (**B**), Bcl-2 (**C**), and Bcl-xl (**D**) protein levels were measured via western blotting 48 h after ultrasound-targeted microbubble destruction (UTMD)-mediated embryonic stem (ES) gene delivery. Endostatin protein levels were significantly higher following cationic microbubble (CMB) delivery of the ES gene compared with the neutral microbubble (NMB), liposome, and control groups. VEGF, Bcl-2, and Bcl-xl protein levels were significantly lower following CMB delivery of the ES gene compared with the NMB, liposome, and control groups (* $p<0.05$ relative to the control and CMB groups, #$p<0.01$ relative to the control group; n=6 per group).

compared with those of the other groups, indicating that the growth of the HRECs in the CMB group had been restrained. Apoptosis was the driving force underlying this phenomenon, resulting in significant cell growth inhibition and cell death. The key elements involved in apoptosis are categorized into two main families of proteins: the Bcl-2 family and the caspase enzymes [27]. As previously reported, endostatin can activate caspase-3 and decrease the Bcl-2 to Bax ratio, thus inducing apoptosis [28]. Therefore, we examined Bcl-2 and Bcl-xl protein levels in HRECs. Detection of Bcl-2 and Bcl-xl in HRECs treated with ES would be indicative of ongoing apoptosis. Western blot analysis and qPCR were employed to detect ES, VEGF, Bcl-2, and Bcl-xl gene expression. The results demonstrated that the ES protein was highly expressed in the CMB group but showed less expression in the other groups. This finding for ES was confirmed at the mRNA level through qPCR analysis. We observed that the apoptosis rates in the CMB group were significantly higher compared with those of the other groups, indicating apoptotic-like cytological changes in the HRECs. Above all, cells successfully transfected with the ES gene induced apoptosis. All of the results confirmed that the treatment effect obtained using CMBs was remarkable in comparison with NMBs or liposomes. ES gene therapy employing UMGD may be an efficient methodology for antiangiogenesis therapy because it can overcome the instability defect associated with ES.

This study demonstrated, for the first time, that ultrasound-targeted cationic microbubble destruction can effectively deliver an ES-GFP plasmid to HRECs. The results indicated that the combination of UTMD with CMBs and ES could be a useful methodology for application in gene therapy targeting neovascularization.

There are recognized limitations of this study. The potential for toxicity, particularly due to the high CMB and DNA doses, is still an obstacle to the application of cationic lipids for gene therapy in vitro and in vivo [22,29]. Furthermore, determining which lipid to use in the generation of CMBs will require additional research. The relationships among the zeta potential, plasmid loading capacity, and transfection efficiency of CMBs also require further investigation.

In conclusion, in this study, CMBs with an increased plasmid carrying capacity were successfully constructed. The transfection efficiency of the CMBs was significantly increased compared with NMBs and liposomes. Due to the increased transfection efficiency, the expression of endostatin was increased following treatment with CMBs, while the expression of VEGF, Bcl-2, and Bcl-xl decreased. Taken together, these data demonstrate the excellent advantages associated with the use of CMBs in enhancing ultrasound-mediated gene transfer in vitro. We propose CMBs as a potential ultrasound contrast agent that may be useful for advancing ultrasound-mediated gene delivery.

ACKNOWLEDGMENTS

This work was supported in part by the National Natural Science Foundation of China Grants: 81,161,120,548, 81,130,025, 81,371,578, 81,371,579, 30,770,565, 81,227,801, 81,170,858 and 61,205,203; the National Key Basic Research (973) Program of China: 2014CB744503; the International S&T Cooperation Program of China: 2014DFG32800; and Program for Innovation Team Building at Institutions of Higher Education in Chongqing 2013(KJTD201303).

REFERENCES

1. Casini G, Dal Monte M, Fornaciari I, Filippi L, Bagnoli P. The β-adrenergic system as a possible new target for pharmacologic treatment of neovascular retinal diseases. Prog Retin Eye Res 2014; 42:103-29. [PMID: 24933041].
2. Wang L, Shi P, Xu Z, Li J. Up-regulation of VEGF by retinoic acid during hyperoxia prevents retinal neovascularization and retinopathy. Invest Ophthalmol Vis Sci 2014; 55:4276-87. [PMID: 24867581].
3. Arpita S. Bharadwaj, Binoy Appukuttan, Phillip A. Wilmarth. Role of the Retinal Vascular Endothelial Cell in Ocular Disease Prog Retin Eye Res 2013; 1:102-80. .
4. Michael S. O'Reilly, Thomas Boehm, Yuen Shing, Naomi Fukai, George Vasios, William S Lane, Evelyn Flynn, James R Birkhead, Bjorn R Olsen, Judah Folkman. Endostatin: an endogenous inhibitor of angiogenesis and tumor growth. Cell 1997; 88:277-85. [PMID: 9008168].
5. Bai YJ, Huang LZ, Zhou AY, Zhao M, Yu WZ, Li XX. Antiangiogenesis effects of endostatin in retinal neovascularization. J Ocul Pharmacol Ther 2013; 29:619-26. [PMID: 23545016].
6. Chen QR, Zhang L, Gasper W, Mixson AJ. Targeting tumor angiogenesis with gene therapy. Mol Genet Metab 2001; 74:120-7. [PMID: 11592809].
7. Xu F, Ma Q, Sha H. Optimizing drug delivery for enhancing therapeutic efficacy of recombinant human endostatin in cancer treatment. Crit Rev Ther Drug Carrier Syst 2007; 24:445-92. [PMID: 18197781].
8. Matsumoto G, Hirohata R, Hayashi K, Sugimoto Y, Kotani E, Shimabukuro J, Hirano T, Nakajima Y, Kawamata S, Mori H. Control of angiogenesis by VEGF and endostatin-encapsulated protein microcrystals and inhibition of tumor angiogenesis. Biomaterials 2014; 35:1326-33. [PMID: 24210874].
9. Zambon L, Honma HN, Lourenco GJ, Saad IA, Mussi RK, Lima CS. A polymorphism in the angiogenesis inhibitor, endostatin, in lung cancer susceptibility. Lung Cancer 2008; 59:276-8. [PMID: 18054814].

10. Taniyama Y, Azuma J, Kunugiza Y, Iekushi K, Rakugi H, Morishita R. Therapeutic option of plasmid-DNA based gene transfer. Curr Top Med Chem 2012; 12:1630-7. [PMID: 23061881].

11. Porter TR, Iversen PL, Li S, Xie F. Interaction of diagnostic ultrasound with synthetic oligonucleotide-labeled perfluorocarbon exposed sonicated dextrose albumin microbubbles. J Ultrasound Med 1996; 15:577-84. [PMID: 8839405].

12. Miller DL, Pislaru SV, Greenleaf JE. Sonoporation: mechanical DNA delivery by ultrasonic cavitation. Somat Cell Mol Genet 2002; 27:115-34. [PMID: 12774945].

13. Kimmel E. Cavitation bioeffects. Crit Rev Biomed Eng 2006; 34:105-61. [PMID: 16749890].

14. Schlicher RK, Radhakrishna H, Tolentino TP, Apkarian RP, Zarnitsyn V, Prausnitz MR. Mechanism of intracellular delivery by acoustic cavitation. Ultrasound Med Biol 2006; 32:915-24. [PMID: 16785013].

15. Nomikou N, Tiwari P, Trehan T, Gulati K, McHale AP. Studies on neutral, cationic and biotinylated cationic microbubbles in enhancing ultrasound-mediated gene delivery in vitro and in vivo. Acta Biomater 2012; 8:1273-80. [PMID: 21958669].

16. Carson AR, McTiernan CF, Lavery L, Hodnick A, Grata M, Leng X, Wang J, Chen X, Modzelewski RA, Villanueva FS. Gene therapy of carcinoma using ultrasound-targeted microbubble destruction. Ultrasound Med Biol 2011; 37:393-402. [PMID: 21256666].

17. Haag P, Frauscher F, Gradl J. Microbubble-enhanced ultrasound to deliver an antisense oligodeoxynucleotide targeting the human androgen receptor into prostate tumours. J Steroid Biochem Mol Biol 2006; 102:103-13. .

18. Tlaxca JL, Anderson CR, Klibanov AL, Lowrey B, Hossack JA, Alexander JS, Lawrence MB, Rychak JJ. Analysis of in vitro transfection by sonoporation using cationic and neutral microbubbles. Ultrasound Med Biol 2010; 36:1907-18. [PMID: 20800945].

19. Nomikou N, Tiwari P, Trehan T, Gulati K, McHale AP. Studies on neutral, cationic and biotinylated cationic microbubbles in enhancing ultrasound-mediated gene delivery in vitro and in vivo. Acta Biomater 2012; 8:1273-80. [PMID: 21958669].

20. Wang DS, Panje C, Pysz MA, Paulmurugan R, Rosenberg J, Gambhir SS, Schneider M, Willmann JK. Cationic versus neutral microbubbles for ultrasound-mediated gene delivery in cancer. Radiology 2012; 264:721-32. [PMID: 22723497].

21. Zhou XY, Liao Q, Pu YM, Tang YQ, Gong X, Li J, Xu Y, Wang ZG. Ultrasound-mediated microbubble delivery of pigment epithelium-derived factor gene into retina inhibits choroidal neovascularization. Chin Med J (Engl) 2009; 122:2711-7. [PMID: 19951601].

22. Panje CM, Wang DS, Pysz MA. Ultrasound-mediated gene delivery with cationic versus neutral microbubbles: effect of DNA and microbubble dose on in vivo transfection efficiency. Theranostics. 2012; 2:1078-91. [PMID: 23227124].

23. Bekeredjian R, Grayburn PA, Shohet RV. Use of ultrasound contrast agents for gene or drug delivery in cardiovascular medicine. J Am Coll Cardiol 2005; 45:329-35. [PMID: 15680708].

24. Chen S, Shohet RV, Bekeredjian R. Optimization of ultrasound parameters for cardiac gene delivery of adenoviral or plasmid deoxyribonucleic acid by ultrasound-targeted microbubble destruction. J Am Coll Cardiol 2003; 42:301-8. [PMID: 12875768].

25. Hernot S, Klibanov AL. Microbubbles in ultrasound-triggered drug and gene delivery. Adv Drug Deliv Rev 2008; 60:1153-66. [PMID: 18486268].

26. Kaneko OF, Willmann JK. Ultrasound for molecular imaging and therapy in cancer. Quant Imaging Med Surg 2012; 2:87-97. [PMID: 23061039].

27. Thornberry NA, Lazebnik Y. Caspases: Enemies within. Science 1998; 281:1312-6. [PMID: 9721091].

28. Ling Y, Lu N, Gao Y. Endostar induces apoptotic effects in HUVECs through activation of caspase-3 and decrease of Bcl-2. Anticancer Res 2009; 29:411-7. [PMID: 19331180].

29. Sakurai F, Nishioka T, Saito H, Baba T, Okuda A, Matsumoto O, Taga T, Yamashita F, Takakura Y, Hashida M. Interaction between DNA-cationic liposome complexes and erythrocytes is an important factor in systemic gene transfer via the intravenous route in mice: the role of the neutral helper lipid. Gene Ther 2001; 8:677-86. [PMID: 11406762].

Articles are provided courtesy of Emory University and the Zhongshan Ophthalmic Center, Sun Yat-sen University, P.R. China. The print version of this article was created on 25 August 2015. This reflects all typographical corrections and errata to the article through that date. Details of any changes may be found in the online version of the article.